combinatorial method for preparing much smaller phosphor libraries, which enabled them to identify some new candidate materials. □

Methods

Powder samples. Europium-doped vanadates of the type $Y_{0.975-n-m}Al_m$ $La_nEu_{0.025}VO_4$ were prepared by firing the well-mixed stoichiometric oxides for 3 h at 1,000 °C, followed by one regrind and one refiring. The brown powders were then stirred in 2 M NaOH for 20 min at 60 °C (to remove unreacted V_2O_5), followed by vacuum filtration and several water washings.

Library processing. Heating and cooling rates varied from 2 °C min⁻¹ to 10 °C min⁻¹. We used this slow thermal cycle to attempt to reduce the complications of thermal stresses which may develop between the films of varying compositions and thicknesses, and the substrate. In spite of such efforts, the film morphology was found to be variable across a library, which is of concern when characterizing relative extrinsic luminescent properties. The large discovery library (Fig. 1a) was heated initially to 500 °C at a rate of 4 °C min⁻¹. After 2 h at 500 °C, it was heated to 850 °C at the same rate and held for 5 h before cooling at 10 °C min⁻¹ to 100 °C. The triangular vanadate library (Fig. 1c) was heated initially to 650 °C at a rate of 2 °C min⁻¹. After 3 h at 650 °C, it was cooled to 100 °C at 2 °C min⁻¹ and removed for initial screening (not shown). The library was then reheated to 900 °C at a rate of 4 °C min⁻¹ and held for 6 h before cooling at 4 °C min⁻¹. The Eu gradient library, which resulted in the data of Fig. 2, was treated similarly.

1. Bunin, B. A., Plunkett, M. J. & Ellman, J. A. The combinatorial synthesis and chemical and biological evaluation of a 1,4-benzodiazepine library. *Proc. Natl Acad. Sci. USA* **91**, 4708–4712 (1994).
2. Xiang, X.-D. *et al.* A combinatorial approach to materials discovery. *Science* **268**, 1738–1740 (1995).
3. Briceño, G., Chang, H., Sun, X., Schultz, P. G. & Xiang, X.-D. A class of cobalt oxide magnetoresistance materials discovered with combinatorial synthesis. *Science* **270**, 273–275 (1995).
4. DiSalvo, F. J. Solid-State chemistry—A rediscovered chemical frontier. *Science* **247**, 649–655 (1990).
5. Maruska, H. P., Parodos, T., Kalkhoran, N. M. & Halverson, W. D. Challenges for flat panel display phosphors. *Mater. Res. Soc. Symp. Proc.* 269–280 (1994).
6. Butler, K. H. *Fluorescent Lamp Phosphors* (Pennsylvania State University Press, University Park, PA, 1980).
7. Vecht, A. phosphors I: Powders. *SID Seminar Lecture Notes* **2**, F-2/3 (1996).
8. Ropp, R. C. *The Chemistry of Artificial Lighting Devices*, 414–656 (Elsevier, Amsterdam, 1993).
9. Blasse, G. & Grabmaier, B. C. *Luminescent Materials* (Springer, Berlin, 1994).
10. Ouweltjes, J. L. Luminescence and phosphors. *Mod. Mater.* **5**, 161–257 (1965).
11. Ozawa, R. & Toshinao, A. Fluorescent elements based on aluminum-substituted yttrium vanadate. Japanese Patent No. 660215. *Chem. Abstr.* **72**, 16741 (1969).
12. Commission Internationale de L'Éclairage *Colorimetry* 2nd edn (Publication CIE No. 15.2, Central Bureau of the Commission Internationale de L'Éclairage, Vienna, 1986).
13. Yokota, W., Shoji, R. & Kimura, K. Yttrium vanadate phosphor. Japanese Patent No. 45041295 B4 701224. *Chem. Abstr.* **75**, 103573 (1970).
14. Thorton, W. A. Quantum efficiency spectra of photoluminescent materials. *J. Electr. Chem. Soc.* **116**, 286–298 (1969).
15. Ropp, R. C. *Luminescence and the Solid State: Studies in Inorganic Chemistry 12* (Elsevier, New York, 1991).
16. Rodgers, J. R. & Villars, P. Trends in advanced materials data—Regularities and predictions. *Mater. Res. Soc. Bull.* **18**, 27–29 (1993).
17. Sun, X.-D, Gao, C., Wang, J. & Xiang, X.-D. Identification and optimization of advanced phosphors using combinatorial libraries. *Appl. Phys. Lett.* **70**, 3353–3355 (1997).

Ordered macroporous materials by emulsion templating

A. Imhof & D. J. Pine

Departments of Chemical Engineering and Materials, University of California, Santa Barbara, California 93106-5080, USA

Ordered macroporous materials with pore diameters comparable to optical wavelengths are predicted to have unique and highly useful optical properties such as photonic bandgaps[1–3] and optical stop-bands[4]. Tight control over the pore size distribution might also lead to improved macroporous materials (those with pores greater than approximately 50 nm) for application as catalytic surfaces and supports[5], adsorbents, chromatographic materials, filters[6], light-weight structural materials[7], and thermal, acoustic[8] and electrical insulators[9]. Although methods exist for producing ordered porous materials with pore diameters less than 10 nm (refs 10, 11), there is no general method for producing such materials with uniform pore sizes at larger length scales. Here we report a new method for producing highly monodisperse macroporous materials with pore sizes ranging from 50 nm to several micrometres. Starting with an emulsion of equally sized droplets (produced through a repeated fractionation procedure[12]), we form macroporous materials of titania, silica and zirconia by using the emulsion droplets as templates around which material is deposited through a sol–gel process[13]. Subsequent drying and heat treatment yields solid materials with spherical pores left behind by the emulsion droplets. These pores are highly ordered, reflecting the self-assembly of the original monodisperse emulsion droplets into a nearly crystalline array[14]. We show that the pore size can be accurately controlled, and that the technique should be applicable to a wide variety of metal oxides and even organic polymer gels.

Our basic idea is to use sol–gel processing to deposit an inorganic material (for example, a metal oxide) at the exterior of the droplets in a monodisperse emulsion. The method takes advantage of the fact that the oil droplets are both highly deformable and easily removable. The high deformability allows the inorganic gel to accommodate large shrinkage, which prevents cracking and pulverization during ageing and drying. Furthermore, droplet volume fractions can exceed the close-packing limit of 74%. As emulsions are made of liquids, the droplets are easily removed by evaporation or dissolution after the templating has been accomplished. The versatility of this technique offers advantages over existing routes for the production of macroporous material, which are limited to widely nonuniform[7] or irregularly shaped pores[15], and therefore do not offer the possibility of ordered porosity. Moreover, other techniques are not readily adapted to produce a wide variety of porous materials.

Sol–gel processes make use of metal alkoxides dissolved in a lower alcohol and hydrolysed by the controlled addition of water. (The alcohol is needed as a solvent because its intermediate polarity makes it a good solvent for both the apolar alkoxide and the polar water.) This produces a sol of nanometre-sized particles of the corresponding metal oxide. Further ageing of the sol at predetermined pH and temperature causes growth and aggregation of the particles resulting in gelation. Drying and heat treatment then produce the metal oxide by removing the solvent and residual organics.

Unfortunately, such a procedure cannot be used to produce most metal oxides in conventional aqueous emulsions. The principal difficulty is that most metal oxides are extremely reactive with water and therefore are incompatible with aqueous emulsions. Another difficulty is that large amounts of alcohol will destroy an emulsion because of its tendency to mix both oil and water. Thus, emulsion templating poses two difficulties: first, to find a stable emulsion in which water is replaced by another polar liquid and second, to find a method to do the sol–gel processing in this polar liquid instead of an alcohol.

In earlier work, we developed several nonaqueous emulsions which are stable against demixing induced by droplet coalescence and against coarsening by Ostwald ripening[16]. Of these, we found that oil-in-formamide emulsions are the most suitable candidates. They can be stabilized by symmetric triblock copolymers of the general formula (ethylene oxides)$_n$–(propylene oxide)$_m$–(ethylene oxide)$_n$ when $2n/m = 0.3$–0.4 and they can be separated into batches consisting of nearly monodisperse droplets using the fractionation procedure referred to above[12]. We also found other nonaqueous emulsions which were not suitable for our purposes because they were destabilized by the sol–gel chemistry.

In our emulsion templating procedure, an oil-in-formamide emulsion is prepared and fractionated to obtain the desired

948

NATURE | VOL 389 | 30 OCTOBER 1997

degree of droplet size uniformity[12]. Next, a metal oxide sol is prepared in pure formamide. This sol is made by mixing a chemically modified metal alkoxide with formamide which contains a little water, such that the resulting metal/water ratio is in the range 3–10. This partially hydrolyses the alkoxide so that it becomes soluble in formamide but does not react further. This eliminates the need for other solvents such as alcohol. At this point, the previously prepared emulsion is dispersed in the sol. The droplet volume fraction is adjusted to the desired porosity by centrifugation. Gelation is induced by adding a small amount of ammonia to increase the pH and takes place over several hours. Before gelation, monodisperse droplets self-assemble into a colloidal crystal when
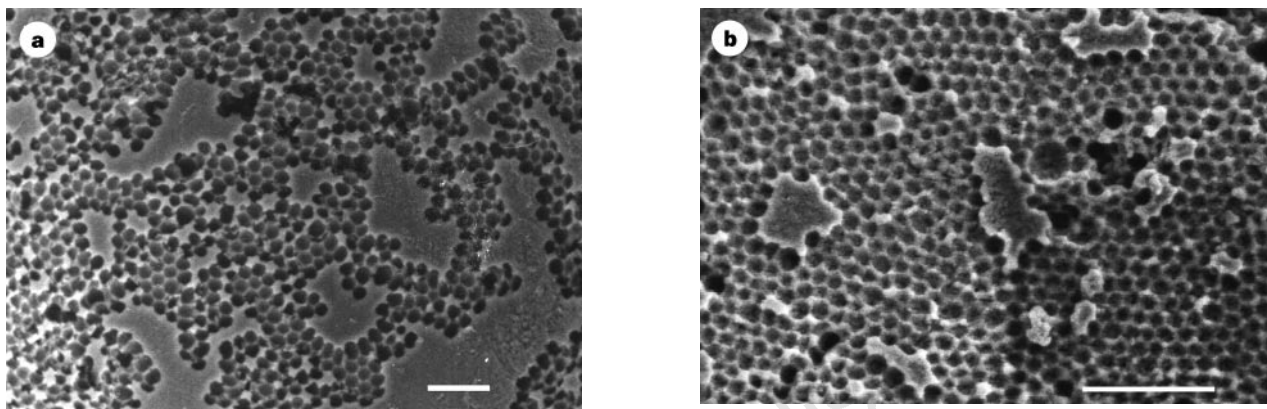
Figure 1 Scanning electron micrographs of porous titania produced in a nearly monodisperse emulsion showing honeycomb structures. The samples had the form of a pellet which was broken to observe the structure inside. **a**, After drying the gel at 60 °C for 2 weeks. The large featureless patches are regions where the pores were not exposed. **b**, The same sample after calcination at 1,000 °C in air for 2 h, showing that the hexagonal pore structure is fully retained. **c**, The structure now consists of small rutile crystallites ~50 nm in size. Scale bars, 1 μm .
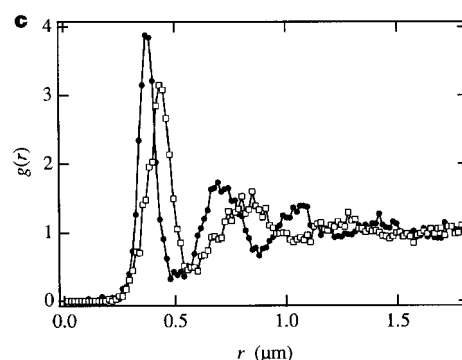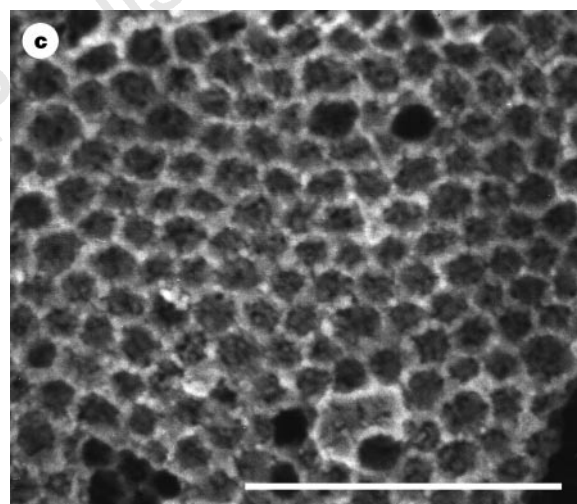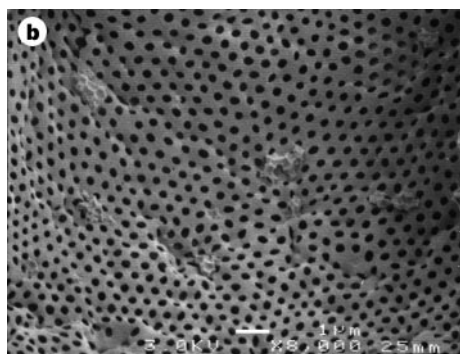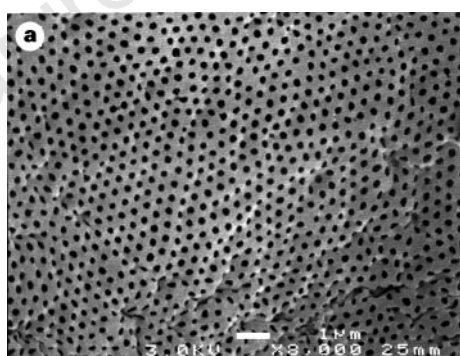
Figure 2 Control over pore size. **a** and **b**, SEM images of porous titania calcined at 1000 °C, prepared from two slightly different emulsion fractions. Although the actual pores are almost touching they do not appear to do so in these images because the surface slices only through the tops of the pores. Scale bars, 1 μm. **c**, Radial distribution functions of the pore centres in the above images, calculated by computer image analysis. They peak at an average inter-pore distance of 0.377 and 0.435 μm, for images **a** (filled circles) and **b** (empty squares) respectively. The half-widths at half-maximum of the first peak are 0.043 and 0.060, respectively. These values are upper limits because the spread in inter-pore distance is increased by the slight buckling of the surfaces seen in the pictures. Note that there are three peaks clearly evident in each of the radial distribution functions (with evidence of a fourth peak) indicating a high degree of local crystalline order.

their volume fraction of droplets exceeds ~50% (ref. 14). The gel is aged to let the reactions go to completion, and then washed in alcohol, dried, and subjected to a heat treatment to remove residual organics.

The pore structure of dried emulsion-templated titania as observed under a scanning electron microscope (SEM) is shown in Fig. 1a. The pores are very uniform with an average diameter of 175 nm and show a high degree of order. The original emulsion had a polydispersity of ~10% and an oil volume fraction of ~55%. During the drying stage the linear dimensions of the gel shrank by ~50%. Thus, the original droplets had a diameter of ~350 nm. After drying, the gel still contains a significant amount of organic material which keeps the metal oxide in an amorphous state. The remaining organics can be removed by heat treatment. SEM images of the same sample after heating at 1,000 °C for 2 h are shown in Fig. 1b, c. Remarkably, the pore structure is fully retained, but the pores have shrunk to 145 nm. X-ray diffraction studies of this material showed the spectrum of TiO₂ crystallized in the rutile structure.

We can exercise considerable control over pore size. In Fig. 2a, b we compare SEM images of porous titania made from two slightly different emulsion fractions. The difference in appearance of these pictures from those of Fig. 1 is caused by the fact that the surface 'decapitated' the pores, whereas in Fig. 1 it cut the pores almost exactly in half. By computer image analysis we obtained the radial distribution function $g(r)$ of the pores (Fig. 2c). This function represents the chance of finding the centre of a pore at a distance r from the centre of another pore, relative to that of a completely homogeneous distribution. The high degree of long-range order is indicated by a series of peaks. The average nearest-neighbour distance is given by the location of the first peak, and the width of this peak is a measure for the spread. These results show that we were able to make materials with a well defined pore size difference of ~20%.

That the macropore structure is unaffected by the heat treatment is all the more remarkable if one considers the changes that take place on a smaller length scale. Detailed analysis of these changes was made on similarly prepared porous titania starting with a nonuniform emulsion. Samples were heated to different tempera-

tures for 2 h and analysed. X-ray powder diffraction spectra showed that between 400 and 800 °C the crystal structure was that of anatase, and that it recrystallized to rutile at higher temperatures. Thermogravimetric analysis showed that 90% of the weight loss takes place below 300 °C. Weight loss is complete at 500 °C when the gels have lost 30–35% of their initial weight. Nitrogen sorption isotherms were measured to investigate the densification of the titania matrix. From the isotherms, the total internal surface area and the total volume of pores smaller than ~50 nm is derived (Fig. 3). The technique is not sensitive to the macropores. The data demonstrate that the titania matrix contained mesopores of 2–10 nm over most of the temperature range (type IV isotherms). Only the sample treated at 1,000 °C had a type II isotherm indicative of a nonporous material. Thus, the data indicate strong densification of the titania matrix. Such control over densification is very useful. In applications such as catalysis and sorption, high porosity and high internal surface area improve efficiency. Macropores facilitate material transport to mesoporous internal regions where reactions can take place. By contrast, for optical applications, it is desirable for the matrix to be as dense as possible to achieve maximal contrast in the refractive index between the matrix and the macropores[3].

One important advantage of our emulsion templating process is that it can be used to produce porous structures in many different materials. This should allow tailoring of their chemical, electrical, magnetic and optical properties. The choice of materials is illustrated by the SEM images of macroporous zirconia and silica, shown in Fig. 4a and b, respectively. In both cases ordered pores were obtained even after calcination at elevated temperatures.

Templating of nonaqueous emulsions is a versatile and inexpensive way of producing ordered macroporous ceramics of many different materials. By using even more monodisperse emulsions, we should be able to make structures, such as those shown in Figs 1 and 2, with even longer-ranged order. Combination with recently developed techniques for nucleating colloidal crystals on surface microstructures[17,18] and for preparing binary alloy structures[19,20]

Figure 3 Effect of calcination temperature on physical properties of porous titania. Figure shows Brunauer–Emmett–Teller specific surface (circles) and mesoporosity (triangles) of titania produced in a polydisperse emulsion plotted versus calcination temperature (2 h in air, heating rate 15 °C min⁻¹). The data were obtained from nitrogen sorption isotherms on a Micromeritics ASAP 2000 adsorption instrument using standard procedures. The mesoporosity is the volume fraction of all pores smaller than 50 nm and therefore does not include the macropores. After calcination at 400 °C both the high mesoporosity (44%) and the large internal surface (208 m² g⁻¹) indicate that the titania matrix is in itself a very open structure. Calcination at 1,000 °C almost completely densifies the matrix.
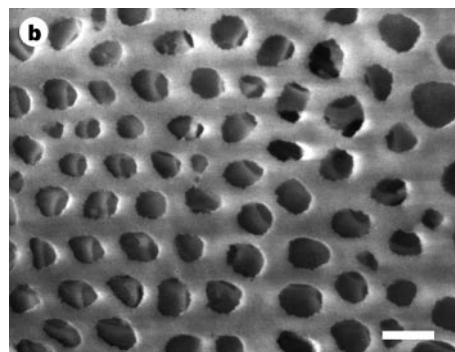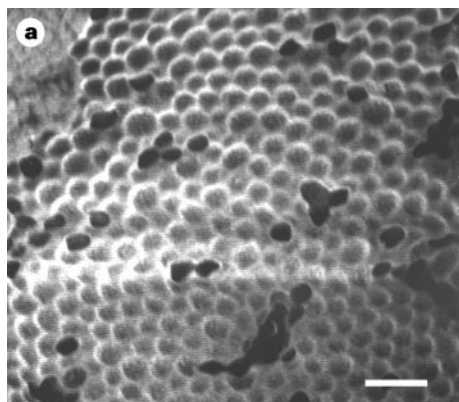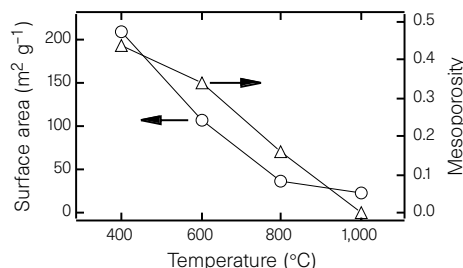
Figure 4 Scanning electron micrographs of emulsion templated materials, showing the applicability of the technique to different materials. **a**, Zirconia with pores of 0.35 μm after heating at 1,000 °C in air for 2 h. **b**, Silica with pores of 1.0 μm after heating at 600 °C for 2 h. The porosity of this sample is 89%, as calculated from the density of the material. As this is above the maximum packing fraction of spheres, the droplets have deformed which resulted in a connected set of pores. This allows one to look some way into the porous structure. Scale bars, 1 μm.

could bring within reach the production of photonic-bandgap materials[4–6] at optical wavelengths. □

Methods

Stable nonaqueous emulsions were obtained with formamide (98%) as the polar liquid and isooctane (>99%) as the oil. Before emulsification, the oil was mixed with ~1% of silicone oil to prevent Ostwald ripening[16]. The surfactant was a symmetric triblock copolymer, poly(ethylene glycol)–poly(propylene glycol)–poly(ethylene glycol) with a relative molecular mass of 5,800 containing 30% by weight of ethylene glycol monomer (Aldrich). Emulsification was done with a homogenizer. The emulsion was fractionated as described by Bibette[12].

The preparation of the ceramic precursor solution is described with the titania synthesis as an example, because it requires the most reactive alkoxide which is the most difficult to handle. Titanium tetraisopropoxide (97%) was treated with an equimolar amount of the chelating agent 2,4-pentanedione to reduce its reactivity towards water[21]. It was then mixed rapidly by stirring with a mixture of water and formamide, such that the resulting H_2O/Ti molar ratio was 3.5 and the Ti concentration was 2.0 M. The resulting clear yellow solution contains a considerable amount of isopropanol produced by the hydrolysis reaction. Because alcohol will destabilize the emulsion, it was removed by double extraction with a fivefold excess of hexanes. The resulting yellow liquid was often turbid. The sol was heated briefly to ~90 °C producing a clear yellow, slightly viscous sol, which did not form a precipitate for several weeks. Zirconia sols were prepared in an analogous fashion, starting with zirconium tetra-n-butoxide (70% in n-butanol). Silica sols were prepared by vigorously mixing silicon tetramethoxide with a mixture of water and formamide acidified to pH 2 with HCl.

The surfactant was dissolved to 2 wt% in the sol. For nonuniform pore materials the oil was emulsified directly into it. For uniform pores the separately prepared monodisperse emulsion was centrifuged and the cream dispersed in the sol. The droplet volume fraction was then set by centrifugation and removal of the clear yellow fluid at the bottom. Then 30% ammonia was added so that the molar ratio NH_3/Ti ≈ 1. The increase in pH induces gelation in about 3 h. Gels were aged at 50 °C for 24 h in closed 2-ml polyethylene vials, then allowed to exchange pore fluids with excess ethanol for 24 h. The gels were then dried at room temperature and calcined in air in a furnace.

1. Yablonovitch, E. Photonic band-gap structures. *J. Opt. Soc. Am. B* **10**, 283–295 (1993).
2. Joannopoulos, J. D., Meade, R. D. & Winn, J. N. *Photonic Crystals: Molding the Flow of Light* (Princeton Univ. Press, 1995).
3. Soukoulis, C. *Photonic Band Gap Materials* (Kluwer, Dordrecht, 1996).
4. Flaugh, P. L., O'Donnel, S. E. & Asher, S. A. Development of a new optical wavelength rejection filter: Demonstration of its utility in Raman spectroscopy. *Appl. Spectrosc.* **38**, 847–850 (1984).
5. Harold, M. P. *et al.* Catalysis with inorganic membranes. *MRS Bull.* **19**, 34–39 (1994).
6. Bhave, R. R. *Inorganic membranes synthesis, characteristics, and applications* (Van Nostrand Reinhold, New York, 1991).
7. Wu, M. X., Fujiu, T. & Messing, G. L. Synthesis of cellular inorganic materials by foaming sol gels. *J. Non-Cryst. Solids* **121**, 407–412 (1990).
8. Litovsky, E., Shapiro, M. & Shavit, A. Gas pressure and temperature dependences of thermal conductivity of porous ceramic materials. 2. Refractories and ceramics with porosity exceeding 30%. *J. Am. Ceram. Soc.* **79**, 1366–1376 (1996).
9. Singer, P. Low k dielectrics: the search continues. *Semicond. Int.* **19**, 88–96 (1996).
10. Beck, J. S. *et al.* A new family of mesoporous molecular sieves prepared with liquid crystal templates. *J. Am. Chem. Soc.* **114**, 10834–10843 (1992).
11. Krauss, T., Song, Y. P., Thoms, S., Wilkinson, C. D. W. & DelaRue, R. M. Fabrication of 2-D photonic bandgap stuctures in GaAs/AlGaAs. *Electron. Lett.* **30**, 1444–1446 (1994).
12. Bibette, J. Depletion interactions and fractionated crystallization for polydisperse emulsion purification. *J. Colloid. Interface Sci.* **147**, 474–478 (1991).
13. Brinker, C. J. & Scherer, G. W. *Sol-Gel Science* (Academic, San Diego, 1990).
14. Pusey, P. N. & van Megen, W. Phase behaviour of concentrated suspensions of hard colloidal spheres. *Nature* **320**, 340–342 (1986).
15. Walsh, D. & Mann, S. Fabrication of hollow porous shells of calcium carbonate from self-organizing media. *Nature* **377**, 320–323 (1995).
16. Imhof, A. & Pine, D. J. Stability of nonaqueous emulsions. *J. Colloid Interface Sci.* (in the press).
17. Dinsmore, A. D., Yodh, A. G. & Pine, D. J. Entropic control of particle motion using passive surface microstructures. *Nature* **383**, 239–242 (1996).
18. van Blaaderen, A., Ruel, R. & Wiltzius, P. Template-directed colloidal crystallization. *Nature* **385**, 321–324 (1997).
19. Hachisu, S. & Yoshimura, S. Optical demonstration of crystalline superstructures in binary mixtures of latex globules. *Nature* **283**, 188–189 (1980).
20. Bartlett, P., Ottewill, R. H. & Pusey, P. N. Superlattice formation in binary mixtures of hard-sphere colloids. *Phys. Rev. Lett.* **68**, 3801–3804 (1992).
21. Sanchez, C., Babonneau, F., Doeuff, S. & Leustic, A. in *Ultrastructure Processing of Advanced Ceramics* (eds Mackenzie, J. D. & Ulrich, D. R.) 77–87 (Wiley, New York, 1988).

Experimental determination of the organic carbon flux from open-ocean surface waters

S. Emerson*, P. Quay*, D. Karl†, C. Winn†, L. Tupas† & M. Landry†

* School of Oceanography, University of Washington, Seattle, Washington 98195, USA

† Department of Oceanography, University of Hawaii, Honolulu, Hawaii 96822, USA

The flux of biologically produced organic carbon from the euphotic zone of the ocean to the deep waters below—the 'biological organic carbon pump'—is one of the main controls on the carbon dioxide partial pressure in the atmosphere[1]. Accurate determination of this flux is therefore critically important for understanding the global carbon cycle and its response to climate change. Our goal is to assess how accurately the biological organic carbon pump can be determined at a single location and to constrain estimates of the global value. As there are no standards against which such environmental fluxes can be measured, we assess accuracy by comparing results from three independent experimental approaches for measuring the net annual export of organic carbon from the euphotic zone in the subtropical North Pacific Ocean near Hawaii. Mass balances of dissolved oxygen, inorganic carbon and organic carbon yield estimates of the organic carbon export flux of 2.7 ± 1.7, 1.6 ± 0.9 and $2.0 \pm 0.9 \, mol \, C \, m^{-2} \, yr^{-1}$, respectively. These three estimates are not significantly different, and establish the present analytically attainable accuracy at this location to be about $\pm 50\%$. If $2.0 \, mol \, C \, m^{-2} \, yr^{-1}$ is typical of the organic carbon export flux in the subtropical ocean, then this vast region, often considered to be a biological desert, may be responsible for up to half of the global-ocean biological organic carbon pump.

The United States JGOFS (Joint Global Ocean Flux Study) Pacific time-series station[2] (station ALOHA of the Hawaii Ocean Time series) is located in the southeastern region of the anticyclonic subtropical gyre at 22° 45′ N, 150° W. Particulate carbon fluxes have been determined over the duration of the programme using drifting sediment traps[3], as have measurements of the dissolved inorganic carbon (DIC) concentration[4] and its stable-isotope ratio[5] ($^{13}C/^{12}C$). Monthly measurements of the concentrations of the gases O_2, N_2 and Ar were made during the years 1990[6], 1992 and 1995.

The biological consumption of DIC (J_{DIC} in $mol \, C \, m^{-2} \, yr^{-1}$) in the euphotic zone of the ocean is equal to the net production of particulate inorganic carbon (PIC) as $CaCO_3$ (J_{PIC}) and organic carbon (J_{OC}) in both dissolved and particulate forms (J_{DOC} and J_{POC}, respectively):

$$J_{DIC} = J_{PIC} + J_{OC} = J_{PIC} + J_{DOC} + J_{POC} \qquad (1)$$

Sediment trap collections and alkalinity/DIC ratios in the upper thermocline[7] at station ALOHA indicate that the flux of PIC out of the upper ocean is only about one-tenth of the total particulate carbon flux; thus, we focus on the net biological production rate of organic carbon, which is stoichiometrically related to the net production of oxygen (J_{O_2}) via the production quotient[8], β:

$$J_{OC} = \beta J_{O_2} \qquad (2)$$

Our approach is to evaluate each of the production terms in these equations by determining mass balances of DIC, oxygen and organic carbon.